Better Geometric Measurements Based on Photometric Information

Lucas J. van Vliet and Piet W. Verbeek

Pattern Recognition Group of the Faculty of Applied Physics
Delft University of Technology
Lorentzweg 1, 2628 CJ Delft, The Netherlands

Abstract — We propose new methods for estimating properties of analog objects in properly sampled multi-dimensional grey-scale images. The finite aperture of lenses ensures bandlimitation of the analog image and allows sampling. Many existing measurement procedures work on a binary object obtained by edge detection and thresholding. The ragged binary edge is disturbed by aliasing which cannot be repaired by smoothing. To solve this problem we propose methods that work directly on the grey-scale image. The grey-scale image contains accurate photometric information. Our new methods yield errors that are generally an order of magnitude better than the traditional binary ones. For applications where a smooth, constant edge height is a prerequisite we introduce *erf-clipping*. Erf-clipping is a point operation that shapes a linear edge region into a scaled error function. In contrast to thresholding it requires very mild oversampling.

1. INTRODUCTION TO SAMPLING-ERROR FREE MEASUREMENTS

The scope of the paper is to propose digital measurements of analog geometric quantities. To facilitate image analysis by computer we need to convert the analog information into a digital representation. The finite aperture of lenses ensures bandlimitation of the analog image and allows sampling. The optical point-spread-function (PSF) can be modeled by a Gaussian of size σ_{psf}. The Nyquist theorem prescribes a minimum sampling rate that allows reconstruction of the analog signal after sampling. To avoid sampling-errors in our measurements we restrict ourselves to use *sampling-error free operators.* A sampling-error free operator is a continuous operation that can be replaced by a cascade of operations: sampling, digital filtering, and interpolation.

A measurement performed on a sampled image that is exactly equal to its analog counterpart is called a *sampling-error free measure* [1]. Envision a signal as a landscape in which the grey-value denotes the elevation. The sum of the grey-value samples *grey-volume* is directly proportional to the volume underneath the landscape.

$$\text{grey-volume}\big(A(x,y,z)\big) = \Delta_x\Delta_y\Delta_z \sum_{i,j,k} A\big(i\,\Delta_x, j\,\Delta_y, k\,\Delta_z\big) \qquad (1)$$

with $A(x,y,z)$ a bandlimited image, Δ_x the sample spacing in the x-direction and $\Delta_x < 2\pi / f_{x,max}$. Thus undersampling up to a factor of two is allowed to obtain an sampling-error free estimate of *grey-volume* [2, 3].

Applying *grey-volume* to photometric data yields the integrated intensity (total energy). To measure the integrated intensity of all objects we need to subtract the background level for all pixel in the image. In case of a perfectly "flat" object, *grey-volume* is proportional to the 2D area or 3D volume of the objects present in the image. For 2D area and 3D volume measurements of "non-flat" objects as well as for all other object measurements we propose an alternative strategy. Transform an input image into output image whose *grey-volume* is directly proportional to quantity to be measured. To avoid aliasing (sampling errors) the transformation should consist of sampling-error free operations. Object properties that can be measured this way are listed in table 1. For practical reasons we focus on measurements in two and three-dimensional images. The transformations use differentiation and nonlinear scaling. Differentiation of D-dimensional images can be achieved by a D-dimensional convolution with a derivative-of-Gaussian filter. For nonlinear scaling of grey-values we introduce *erf-clipping* which replaces thresholding by a sampling invariant operation.

Table 1: Overview of object measurements in multi-dimensional signals. The column "feature" denotes the dimensionality of the measure in D-dimensional space. In addition to D spatial coordinates we have one grey-value per sample point.

Feature	2D	3D	*D*D
grey-volume	integrated grey-value	integrated grey-value	integrated grey-value
size D+1	mass, energy	mass, energy	
size D	area	volume	hyper-volume
size D–1	edge length	surface area	hyper-surface
size D–2		length	hyper-length
size D–3			hyper-(D–3 size)
shape D–3	bending energy	bending energy	
shape 0	Euler number	Euler number	Euler number

2. NONLINEAR SCALING: ERF-CLIPPING

Nonlinear scaling of the photometric data (grey values) is applied to obtain a "flat" object. Well-known scaling functions are thresholding $S_{threshold}$ and hard-clipping $S_{hard\text{-}clipping}$. Scaling a sampled image is equivalent to scaling the continuous image and sampling. Thresholding and hard-clipping distort the grey value landscape so that it is no longer bandlimited. To solve this problem we introduce a soft-clipping technique called erf-clipping.

$$S_{thresholding}(g,t,r) = \begin{cases} t + \tfrac{1}{2}r & \text{for } g \geq t \\ t - \tfrac{1}{2}r & \text{for } g < t \end{cases}$$

$$S_{hard\text{-}clipping}(g,t,r) = \begin{cases} t + \tfrac{1}{2}r & \text{for } g \geq t + \tfrac{1}{2}r \\ g & \text{for } t - \tfrac{1}{2}r < g < t + \tfrac{1}{2}r \\ t - \tfrac{1}{2}r & \text{for } g \leq t - \tfrac{1}{2}r \end{cases} \qquad (2)$$

$$S_{erf\text{-}clipping}(g,t,r) = t + \tfrac{1}{2}r\,\mathrm{erf}\left(\sqrt{\pi}(g-t)r^{-1}\right)$$

with g the input signal, t the "threshold" level, and r the so called clip range. Instead of shaping a rising input signal into a step edge (thresholding) or a ramp edge (hard-clipping), erf-clipping shapes a linear rising input signal into a scaled error function (c.f. figure 1). All scaling methods cross the "threshold" level t in one point. In contrast to thresholding, both hard-clipping and erf-clipping preserve the slope of the signal around the selected "threshold".

The short space spectra (in analogue to the short time spectrum in speech recognition) of the output signals after a scaling applied to a linear region of the signal are:

$$\mathcal{F}\{S_{thresholding}\} \approx \frac{1}{2\pi i f} + \pi\delta(f) \approx \frac{1}{2\pi f} \qquad (3)$$

$$\mathcal{F}\{S_{hard\text{-}clipping}\} \approx \frac{\sin(2\pi T f)}{2\pi T f}\left(\frac{1}{2\pi i f} + \pi\delta(f)\right) \approx \left(\frac{1}{2\pi f}\right)^2 \qquad (4)$$

$$\mathcal{F}\{S_{erf\text{-}clipping}\} \approx \exp\left(-2\pi^2\sigma^2 f^2\right)\left(\frac{1}{2\pi i f} + \pi\delta(f)\right) \approx \frac{\exp\left(-2\pi^2\sigma^2 f^2\right)}{2\pi f} \qquad (5)$$

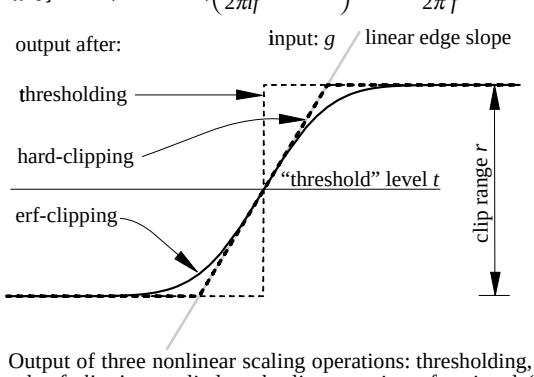

Figure 1: Output of three nonlinear scaling operations: thresholding, hard-clipping, and *erf-clipping* applied to the linear region of a signal (linear edge slope).

0-7803-1880-3/94/$4.00 © 1994 IEEE

We notice that the Fourier transform of the thresholded signal decays slowly ($\propto f^{-1}$), the signal after hard-clipping somewhat faster ($\propto f^{-2}$), whereas the bandwidth of erf-clipped signal is mainly determined by the approximate bandwidth of the underlying Gaussian. Figure 2 shows the Fourier transform of the output signals after thresholding, hard-clipping and erf-clipping. The erf-clipping result corresponds to a Gaussian filtered step edge. The size of the Gaussian filters is similar to the size of the analog prefilter (PSF) when sampled at the Nyquist rate, σ_{psf}= 0.9 pixels [2].

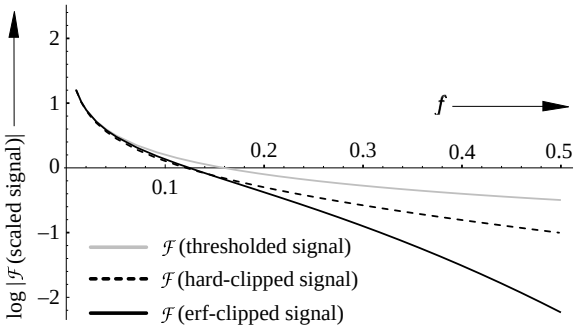

Figure 2: The Fourier transform of the signals after thresholding, hard-clipping and erf-clipping. The erf-clipping result corresponds to a Gaussian filtered step edge. The size of the Gaussian filters is similar to the size of the PSF, σ_{psf} = 0.9.

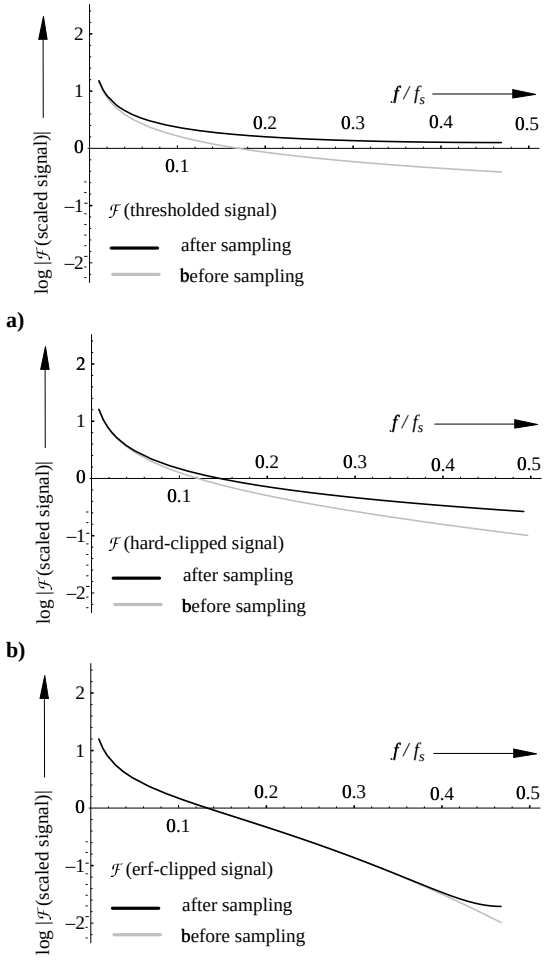

Figure 3: The Fourier transforms of the scaled signals before (grey lines) and after (black lines) sampling. The difference between the line pairs is due to aliasing. **a)** spectrum after thresholding, **b)** spectrum after hard-clipping, **c)** spectrum after erf-clipping.

From figure 2 we may conclude that erf-clipping produces a signal that is approximately bandlimited, whereas thresholding and hard-clipping produce signals with considerable energy contributions at half the sampling frequency, $\pm\frac{1}{2}f_s$.

Figure 3 shows the Fourier transforms of the scaled signals before (grey lines) and after (black lines) sampling. The difference is due to aliasing. It is clear that the spectrum of the erf-clipped signal (figure 3c) is almost completely preserved whereas the entire spectra of the signals after thresholding and hard-clipping are heavily corrupted due to aliasing.

When erf-clipping replaces thresholding it is often applied to a raw intensity image or a second derivative filtered image. The first leaves us with choices for the central isophote ("threshold" level *t*) and the clip range *r*, whereas the latter is usually applied around the zero-crossing and leaves us with a choice for the clip range. In [3] we proposed to set the clip range at roughly 1/4 of the original edge height. In [3] we also showed that *erf-clipping* increases the bandwidth of the signal. The increase is roughly the ratio between the edge height (contrast) before and after clipping.

3. ZERO CROSSING POSITION OF CURVED EDGES

There exists an extensive literature on edge detection techniques and the evaluation of edge detectors in the presence of noise. The so-called stochastic errors have received a lot of attention while the systematic errors and sampling issues have been neglected. Berzins [4] paid some attention to edge location errors near corners.

Analog and digital low-pass filters yield systematic errors in the zero-crossing position of curved edges after second derivative filtering. The filters studied are: the Laplacian-of-Gaussian (LoG), the second derivative in gradient direction (SDGD) and their sum PLUS. The zero-crossing of a second derivative filter is a well-known edge localization criterion. In previous work [5, 6] we have shown that all derivative based edge detectors exhibit a systematical error in their zero-crossing position that cannot be avoided. The blurring of curved edges – optical as well as digital – exerts an influence on the edge location. This discovery of this phenomenon has driven us to investigate the behavior of these systematic errors as function of the edge radius and the size of the low-pass filter. We found that two well-known edge detectors: the LoG and the SDGD produce an equal edge shift, but in opposite direction. The zero-crossing of a convex edge is displaced outwards by the LoG and inwards by the SDGD. A newly proposed edge detector called PLUS (PLUS = LoG + SDGD) yields an edge displacement that is an order of magnitude smaller than the ones produced by either of its constituents (c.f. table 1). Accurate prediction of the edge shifts requires that the sampling requirements are satisfied and that the size of the overall smoothing (σ_{total}) remains a few times smaller than the edge radius R ($2\sigma_{total}<R$). In [5] we have shown that SDGD and PLUS require three times oversampling to avoid aliasing.

Table 1: Relative location error $(r_0-R)/R$ of constant curvature edges as function of the total σ ($\sigma^2=\sigma_{slope}^2+\sigma_{PSF}^2+\sigma_{smooth}^2+\sigma_{derivative}$) and the object radius R. The positive axis is defined from the center of the object. The sampling requirement is given as well.

filter	sampling	$\frac{(r_0-R)}{R}$ in 2D	$\frac{(r_0-R)}{R}$ in 3D
SDGD	≥ 3x Nyquist or $\sigma \geq 2.7$	$\approx -\frac{1}{2}\left(\frac{\sigma}{R}\right)^2$	$\approx -1.0\left(\frac{\sigma}{R}\right)^2$
Laplace	≥ 1x Nyquist	$\approx \frac{1}{2}\left(\frac{\sigma}{R}\right)^2$	$\approx 1.0\left(\frac{\sigma}{R}\right)^2$
PLUS	≥ 3x Nyquist or $\sigma \geq 2.7$	$\approx \frac{1}{2}\left(\frac{\sigma}{R}\right)^4$	$\approx 1.0\left(\frac{\sigma}{R}\right)^4$

An alternative method for edge localization uses a linear combination of Gaussians. A Doublet-of-Gaussians filter is similar to a Laplacian-of-Gaussian (LoG). A combination with N Gaussians reduces the edge shift to a fraction $(1/(2N-3))$ of the one produced by a LoG filter [5, 6]. Smoothing by a Gaussian filter also displaces the isophotes. The isophotes at half edge height is displaced inwards by the same amount as the SDGD zero crossing. In [7] we extended the 2D algorithm for isophote curvature estimation to measure the principal curvatures of an isophote surface patch.

4. AREA OR VOLUME, PERIMETER OR SURFACE-AREA, SPAGHETTI LENGTH, EULER NUMBER AND BENDING ENERGY,

For images that contain a single object the global measures produce object features. Our grey-scale measurements transform the input image into an output image. The *grey-volume* – sum of the sample values – of the output image is directly proportional to the required measure. Using this principle we developed 2D estimators for area, contour length, Euler number, and bending energy of a thin rod. In 3D we developed estimators for volume, surface area, spaghetti length, Euler number and the bending energy of a thin plate.

All our object measurements depend on the contour or surface of the analog object. Knowledge about the behavior of (curved) object edges due to low-pass filtering is a first requirement to construct unbiased estimators. Another vital element is *erf-clipping*. This form of nonlinear scaling is used to flatten the grey landscape. Wherever possible we have compared our results to those of others. By doing so, one difficulty remains. All authors who have published measurement errors started from a point sampled version of an analytical object description. They have neglected to model the imaging process. Their reported errors are optimistic since they omit systematic error contributions due to low-pass filters in the imaging process and they avoid all errors related to edge localization.

4.1. 2D area & 3D volume

Traditional methods produce a binary object whose area or volume is estimated by pixel or voxel counting. We use the zero crossing of our PLUS operator to denote the object boundaries. PLUS is constructed from partial derivatives with a built-in Gaussian of size $\sigma = 3.0$. From here we followed two strategies. The first produces a binary image by thresholding at level zero and filling the interior of the object. Counting the number of object pixels or voxels yields a measure for area or volume. The second alternative applies *erf-clipping* in the linear edge region around the zero crossing with clip range $r=h/4$, where h denotes the edge height in the image or the dynamic range after PLUS filtering prior to clipping. Afterwards, the upper clipping level is propagated inwards whereas the lower clipping level is propagated into the background resulting in a flat object (upper clipping level) on a flat background (lower clipping level). This yields the grey-scale landscapes A_{2D} or V_{3D}. The resulting *grey-volume* of A_{2D} or V_{3D} is proportional to the area or volume of the underlying object. Erf-clipping produces an erf-shaped edge profile (anti-symmetric) centered around the zero crossing and of a width w described by the standard deviation of a Gaussian. For a curved edge there is more additional "mass" outside the contour than there is missing inside the contour. The resulting positive bias term for simply-closed objects is πw^2 in 2D and $4\pi w^2 R$ in 3D [5, 6]. In 2D the clip-width bias is constant and can be subtracted to obtain an area estimation limited by the accuracy of the PLUS operator. In 3D we either use two clip ranges ($r=h/4$ and $r=h/5$) to eliminate the erf-width bias or we use a linear combination of 1.0 Laplace + 1.07 SDGD (instead of PLUS) as second derivative filter to compensate the erf-width bias.

Table 2: Overview of 2D area and 3D volume estimation methods. The PLUS bias and erf-width bias are absolute bias terms, bias* is the relative bias after correction. PLUS uses Gaussian derivatives with $\sigma = 3.0$. The clip range is 1/4 of the PLUS range.

Method	bias terms		relative errors after correction	
	PLUS bias	erf width bias	bias* (%) $R\in(10\rightarrow50)$	CV (%) $R\in(10\rightarrow50)$
2D: binary method	$\pi\sigma^4/R^2$	πw^2	$1\rightarrow10^{-3}$	10^{-3}
2D: grey-scale method	$\pi\sigma^4/R^2$		$1\rightarrow10^{-2}$	10^{-2}
3D: binary method	$4\pi\sigma^4/R$	$4\pi w^2 R$	$1\rightarrow10^{-3}$	10^{-3}
3D: grey-scale method	$4\pi\sigma^4/R$		$1\rightarrow10^{-2}$	10^{-2}

Thus, the erf-width bias can be compensated. The corrected (*) grey-scale method produces a bias smaller or equal to the one produced by the binary method. The bias decreases from 1% for object radii around 10 pixels to 10^{-3} % for object radii around 50 pixels. The CV of the grey-scale method is an order of magnitude smaller than the CV of the binary method. For an overview see table 2.

4.2. 2D perimeter & 3D surface area

Traditional methods assign weights to the various pixels configurations along a binary contour in 2D [8, 9] or over a binary surface in 3D [10]. Summation of the weighted contour pixels or surface voxels yields the perimeter or surface area estimate. In our grey-scale method the boundary of the object is transformed into a landscape L_{2D} or A_{3D} whose *grey-volume* is proportional to its contour length or surface area. The contour can either be an isophote in the raw data or the zero crossing after second derivative filtering.

The isophote method applies *erf-clipping* to a linear edge region producing a flat grey landscape with erf-shaped edge profiles. The modulus of a gradient (implemented using Gaussian derivatives) yields a Gaussian distribution shifted inwards for convex edges (the edge shift is exactly equal to the one produces by the SDGD). This landscape is called $L_{2D\_isophote}$ or $A_{3D\_isophote}$. The shift causes a negative bias term that can be partially compensated for in 3D, but not in 2D [2, 3].

The zero-crossing method uses a more appropriate edge definition that does not suffer from shading. The Laplacian-of-Gaussian (LoG) yields a zero-crossing that is shifted outwards for convex edges. Applying the isophote method to the Laplacian zero-crossing, the LoG bias and the gradient bias ($\sigma_{grad}^2 = \sigma_{psf}^2 + \sigma_{LoG}^2$) cancel each other. This yields a Gaussian cross-section at the exact edge location. Such a landscape is called $L_{2D\_zero\text{-}crossing}$ or $A_{3D\_zero\text{-}crossing}$. The finite width of the Gaussian profiles along the object boundary produces a small positive bias in 3D images. This bias term, however, is independent of the object shape and size and can easily be subtracted from the surface area estimate [2, 3].

Table 3: Overview of 2D edge length and 3D surface area estimation methods. The edge shift bias and edge thickness bias are absolute bias terms, bias* is the performance after bias correction. The isophote method uses $\sigma_{grad} = 1.5$ whereas the zero crossing method uses $\sigma_{LoG} = 1.5$, a clip range of 1/4 of the Laplace range and $\sigma_{grad} = 1.75$ (only when the images are sampled exactly at the Nyquist rate). Due to erf-clipping over 1/4 of the input range $w^2 << \sigma^2$.

Method	bias terms		relative errors after correction	
	edge shift (disc/sphere)	edge thickness	bias* (%) $R\in(10,50)$	CV (%) $R\in(10,50)$
2D: isophote length	$-\pi\sigma^2/R$	0	$10\rightarrow10^{-1}$	$10^{-2}\rightarrow10^{-4}$
2D: zero crossing length	0	0	$10^{-1}\rightarrow10^{-2}$	$10^{-2}\rightarrow10^{-3}$
3D: isophote area	$-8\pi(\sigma^2+\sigma_{psf}^2)$	$4\pi(\sigma^2+w^2)$	$1\rightarrow10^{-2}$	$10^{-1}\rightarrow10^{-3}$
3D: zero crossing area	0	$4\pi(\sigma^2+w^2)$	$1\rightarrow10^{-3}$	$10^{-1}\rightarrow10^{-3}$

Table 3 shows the relative bias (*) and CV after bias correction for both methods. Experiments show that unbiased estimators for 2D edge length and 3D surface area can be constructed. Comparing our method with existing binary methods [8, 9] we notice that: 1) our bias is almost everywhere an order of magnitude smaller; 2) our CV's in 2D are more than an order of magnitude smaller and our CV's in 3D are two or three orders of magnitude smaller. We may conclude that proper sampling really pays off. Moreover, our method takes care of edge shifts by optical smoothing (σ_{PSF}).

Other experiments showed that some undersampling does not sacrifice the performance of our method. Sampling at the Nyquist rate σ_{psf}=0.9, derivative-of-Gaussian with σ_{grad}=1.5 (isophote method) or sampling at the Nyquist rate σ_{psf}=0.9, LoG with σ_{LoG}=1.5 and derivative-of-Gaussian with σ_{grad}=1.75 (zero crossing method), the measurement procedures perform well.

4.3. 3D length

Others have extended the binary methods for length estimation in 2D to 3D methods for measuring the length of binary space curves [11, 12, 13]. The three possible transitions: grid parallel, square diagonal, and cube diagonal are properly weighted and summed to produce an unbiased minimum-MSE length estimate.

Here we estimate the length of 3D space curves through *grey-volume* measurements. To transform a 3D cylinder into a *grey-volume* proportional to its length requires a second derivative perpendicular to the center line of the cylinder, thus in the radial direction. The second derivative in gradient direction (SDGD) accomplishes this. Thus the integrated SDGD yields a

grey-volume proportional to the length of the cylinder. The method requires a constant line intensity along the line. This can be accomplished by applying *erf-clipping* to the slopes of the lines. The proposed method is independent of the line diameter and hence insensitive to the "threshold" level around which *erf-clipping* is applied. The length contribution is virtually independent of the orientation of the line. We have tested our method in randomly oriented cylinders of radius 20 sampled at the Nyquist rate. The SDGD uses Gaussian derivatives of size $\sigma_{SDGD} = 1.35$. Table 4 shows that the errors are three orders of a magnitude smaller than the ones reported by Verwer [11] for the 3x3x3 chamfer method.

Table 4: Error comparison between two 3D length estimators: Verwer's [11] 3x3x3 chamfer method and our integrated SDGD.

Error	3D chamfer method	integrated SDGD
bias	0.00 %	0.00 %
CV	2.30 %	$2.1\ 10^{-3}$ %
maximum error	2.95 %	$4.7\ 10^{-3}$ %
minimum error	–10.60 %	$-3.2\ 10^{-3}$ %

We can measure the length of spaghetti (not necessarily of constant width). The length of macaroni, however, remains an unsolved problem. The inside tube gives a virtual negative contribution producing a length of macaroni equal to zero. This can be explained by the theory on Euler numbers.

4.4. Euler number

We have proposed and tested two methods for estimating Euler numbers in two dimensions. The first is deduced from the 3D length estimator. The integrated second derivative in the gradient direction yields a 2π contribution for every simply-closed object in 2D images. A hole yields a contribution of -2π. The bias is around 1%. The second method is derived from the field of differential geometry. The integrated curvature of SCC objects always produces 2π per revolution [14]. Around holes the curvature has an opposite sign and results in an integrated curvature of -2π. This method has a bias of 0.1%, a smaller bias in exchange for a more complex algorithm [2].

In three dimensions we have only one method. Again from differential geometry we know that the surface integral of the Gaussian curvature yields 4π for each SCC object (Gauss-Bonnet formula [15]). Each tunnel (handle) through the object contributes -4π. Unfortunately, we cannot discriminate between surfaces around objects and around holes. The bias is again smaller than 0.1% [2].

4.5. Bending energy

From the theory of elasticity we know that the bending energy of an object formed from flexible straight or flat material represents the energy stored in its shape. Our 2D bending energy is directly proportional to the bending energy of a deformed circular rod [16]. In 3D the bending energy corresponds to that of a deflected thin plate. The bending energy per unit length is the curvature squared κ^2, per unit surface area it is the sum of the squared principal curvatures $\kappa_1^2 + \kappa_2^2$ [7] The integration of the bending energy contributions over the object boundary is realized by a multiplication with the landscape $L_{2D\_zero\text{-}crossing}$ or $A_{3D\_zero\text{-}crossing}$ (perimeter or surface area estimator). This way the contour or surface area is locally weighted by its energy contribution. The resulting *grey-volume* yields the desired bending energy. Thus, the combination of isophote curvatures and perimeter or surface area estimators allows us to measure the bending energy. Typical error for discs and ellipses in 2D and spheres and ellipsoids in 3D are given in table 5.

Table 5: Overview of 2D and 3D bending energy estimation. The isophote curvatures are calculated using Gaussian derivatives of $\sigma_\kappa = 5.4$ for the discs and spheres and $\sigma_\kappa = 3.8$ for the ellipses and ellipsoids. The GCL landscape uses a $\sigma_{LoG} = 1.5$, a clip range of 1/4 of the Laplace range and $\sigma_{grad} = 1.75$. All images were sampled at the Nyquist rate.

Object	bias (%)	CV (%)
discs of $R \in (15,100)$	$3 \rightarrow 10^{-1}$	10^{-3}
ellipses of eccentricity $\in (1,0.3)$, R_{min}=16.2	$2 \rightarrow -1$	10^{-3}
spheres of $R \in (15,45)$	10^{-2}	10^{-3}
ellipsoids of eccentricity $\in (1,0.7)$, R_{min}=11.4	10^{-2}	10^{-3}

5. CONCLUSIONS

We presented sampling-error free measurements that are better (lower bias and lower coefficient-of-variation CV = μ/σ) than the traditional binary methods. The sum of samples *grey-volume* can easily be measured without a sampling error. All geometric properties of single objects are measured as follows. Transform an input image into output image whose *grey-volume* is directly proportional to quantity to be measured. To avoid aliasing (sampling errors) the transformation should consist of sampling-error free operations. Using this principle we developed 2D estimators for area, contour length, Euler number, and bending energy of a thin rod. In 3D we developed estimators for volume, surface area, spaghetti length, Euler number and the bending energy of a thin plate.

In the above methods we take edge displacement due to optical as well as digital blurring into account. To separate object from background we applied milder *erf-clipping* rather than the very nonlinear threshold operator.

6. ACKNOWLEDGMENTS

This work was partially supported by the Dutch Government as part of the SPIN-3D program for 3D biomedical image analysis, the SPIN-FLAIR II program "Delft Intelligent Assembly Cell", The Netherlands Foundation for Biomedical Research NWO-MEDIGON, grant 900-538-016, and Imagenetics (Naperville, Illinois, USA).

7. REFERENCES

[1] P.W. Verbeek, "A class of sampling–error free measures in oversampled band–limited images," Pattern Recognition Letters, **3**, pp. 287–292, 1985.

[2] L.J. van Vliet, "Grey-Scale Measurements in Multi-Dimensional Digitized Images," Ph.D. thesis, Delft University Press, Stevinweg 1, Delft, The Netherlands, 1993.

[3] P.W. Verbeek and L.J. van Vliet, "Estimators of 2D edge length and position, 3D surface area and position in sampled grey-valued images," BioImaging, **1**(1), pp. 47-61, 1993.

[4] V. Berzins, "Accuracy of Laplacian edge detectors," Computer Vision, Graphics and Image Processing, **27**, pp. 195–210, 1984.

[5] P.W. Verbeek and L.J. van Vliet, "On the location error of curved edges in low-pass filtered 2D and 3D images," IEEE Transactions on Pattern Analysis and Machine Intelligence, submitted 1992, in press.

[6] L.J. van Vliet and P.W. Verbeek, "Object Localization using MoG Filters: Multiple-of-Gaussians," Pattern Recognition Letters, submitted 1993, in press.

[7] L.J. van Vliet and P.W. Verbeek, "Curvature and bending energy in digitized 2D and 3D images," 8th SCIA Scandinavian Conference on Image Analysis, Tromsø, Norway, pp. 1403-1410, 1993.

[8] A.M. Vossepoel and A.W.M. Smeulders, "Vector code probabilities and metrication error in the representation of straight lines of finite length," Computer Graphics and Image Processing, **20**, pp. 347–364, 1982.

[9] L. Dorst and A.W.M. Smeulders, "Length estimators for digitized contours," Computer Vision, Graphics and Image Processing, **40**, pp. 311–333, 1987.

[10] J.C. Mullikin and P.W. Verbeek, "Surface area estimation of digitized planes," BioImaging, **1**, pp. 6-16, 1993.

[11] B.J.H. Verwer, "Local distances for distance transformations in two and three dimensions," Pattern Recognition Letters, **12**, pp. 671-682, 1991.

[12] A.L.D. Beckers and A.W.M. Smeulders, "Optimization of length measurements for isotropic distance transformations in three dimensions," CVGIP: Image Understanding, **55**(3), pp. 296-306, 1992.

[13] N. Kiryati and O. Kübler, "On chain code probabilities and length estimators for digitized three dimensional curves," 11th IAPR International Conference on Pattern Recognition, The Hague, The Netherlands, pp. 259-262, 1992.

[14] H. Hopf, "Über die drehung der tangenten und sehnen ebenen kurven," Comp. Math., **2**(S), pp. 50-62, 1935.

[15] J.J. Stoker, "Differential Geometry," Wiley-Interscience, 1969.

[16] I.T. Young, J.E. Walker , and J.E. Bowie, "An analysis technique for biological shape I," Info Control, **25**, pp. 357-370, 1974.